Macroscopic theory of pulsed-laser annealing. II. Dopant diffusion and segregation

R. F. Wood, J. R. Kirkpatrick,* and G. E. Giles*
Solid State Division, Oak Ridge National Laboratory, Oak Ridge, Tennessee 37830
(Received 31 October 1980)

The radiation from *Q*-switched ruby and Nd:YAG (yttrium aluminum garnet) lasers can anneal the lattice damage produced by ion implantation of semiconductors. In the first paper of this series, we described the models and methods we have been using for heat-transport calculations during pulsed-laser annealing and gave numerous illustrations of the type of results which are obtained. In this paper, we discuss dopant-diffusion calculations in detail, with particular emphasis on the incorporation of segregation effects into the modeling. From the forms of the experimental dopant profiles, it is established that pulsed-laser annealing is a nonequilibrium process, but in this paper the interface segregation coefficient is treated as an adjustable parameter and no attempt is made to justify the values obtained. Approximate analytical and finite-difference solutions to the diffusion equation are discussed and compared. It is argued here that the excellent fit between theory and experiment which is obtained is a strong indication of the basic validity of the melting model of pulsed-laser annealing.

I. INTRODUCTION

This is the second in a series of papers on the macroscopic theory of pulsed-laser annealing. In the first paper,[1] referred to as I or Paper I in the following, we discussed the physical and mathematical models we have used recently for calculations of heat generation and transport during pulsed-laser annealing of ion-implanted silicon[2]; extensive results of the calculations were given. Those results showed that for sufficiently energetic laser pulses the near surface region melted and stayed molten to a depth of approximately 0.5 μm for periods of the order of 100 nsec. Very high recrystallization velocities of the order of 4 m/sec were calculated. We have previously shown that results of the thermal calculations, when combined with calculations of dopant diffusion in the *molten* material, can explain the observed spreading of dopant profiles in ion-implanted laser-annealed samples[2] and samples on which a doped amorphous layer has been recrystallized by the laser radiation.[3]

Although some results of dopant diffusion calculations have been given in the papers of Ref. 2, we have not yet discussed the calculations in detail. In this paper, we supply the details which have been missing from the previous papers and give extensive new results. Dopant diffusion during recrystallization of a laser irradiated sample is a moving-boundary problem[4] and cannot be solved exactly except in special cases. Approximate analytical and finite difference solutions are discussed and compared, and the incorporation of segregation effects into the modeling is emphasized. Results of the calculations are compared to the extensive body of experimental data obtained over the past few years at Oak Ridge National Laboratory (ORNL).[5] The excellent agreement between theory and experiment which is obtained is a strong indication of the basic validity of the melting model of pulsed-laser annealing.

The paper is arranged into five sections. In the next section, the well-developed theory of dopant segregation during crystallization of a molten semiconductor containing a uniform concentration of dopants is reviewed. In Sec. III, the models we have used in our dopant redistribution and segregation calculations are presented and discussed. Section IV contains most of the numerical results and some discussion of them. Additional discussion of the results, as well as some concluding remarks about the calculations and about the melting model of pulsed-laser annealing, are given in the last section.

II. REVIEW OF THE MACROSCOPIC THEORY OF SEGREGATION

In this section we give a brief review of the macroscopic theory of segregation for an impurity (solute) which initially has constant concentration in a molten solvent. By a macroscopic theory we mean one that does not inquire about the details of atomic processes going on in the interface region between the liquid and solid. In fact, here the interface region is assumed to be infinitely thin and the information about processes at the interface is contained entirely in the interface segregation (or distribution) coefficient. This quantity is defined as the ratio of the

concentrations of the impurity in the solid C_s to its concentration in the liquid C_l immediately in front of the interface. It is important to distinguish carefully between the interface segregation coefficient k_i and the effective segregation coefficient k_{eff}. This latter quantity is generally defined as the ratio of the impurity concentration in the solid to the initial constant impurity concentration C_0 in the liquid solute. Thus, for k_i and k_{eff} we have

$$k_i = C_s/C_l \ , \tag{1}$$

$$k_{\text{eff}} = C_s/C_0 \ . \tag{2}$$

In addition to these quantities, a number of other "segregation coefficients" appear in the literature. We will reserve the symbol k_i^0 for the interface segregation coefficient when crystal growth occurs so slowly that a condition of quasithermodynamic equilibrium is maintained at all times. Burton, Prim, and Slichter[6] have given the equation

$$k = \frac{k'}{k' + (1-k')\exp(-v\delta/D_l)} \tag{3}$$

for an "effective distribution coefficient." In this equation, k' can be either k_i or k_i^0, v is the melt-front velocity, D_l is the diffusion coefficient in the liquid, and the rather arbitrary quantity δ is sometimes referred to as the diffusion boundary layer thickness. This equation has caused a great deal of confusion because it apparently gives a relationship between k and k' in terms of the melt-front velocity, and this has led some to conclude that it applies to the laser-annealing process. In fact, Eq. (3) applies to Czchrolski-type growth of crystals in which the rotational velocity of the growing crystal is nonzero; it has little or no direct relationship with the situation encountered in laser annealing. One of the primary purposes of this section is to clarify the physics underlying the various segregation coefficients appearing in the literature. To do this, we will first consider one-dimensional solidification in which only diffusion of an impurity in the liquid is important and we will then discuss the paper of Burton *et al.*

A. One-dimensional solidification without convection

There are many treatments of this topic in the literature but we have found the development given by Smith, Tiller, and Rutter[7] particularly useful and will follow it here. It is assumed that the solidification is unidirectional (x direction) with a constant liquid-solid interface (melt-front) velocity v. The concentration of the solute in the solvent is initially uniform and has value C_0. It is further assumed that: (i) impurity diffusion in the solid is negligible; (ii) no convective mixing of solute and solvent occurs; (iii) the interface distribution or segregation coefficient k_i is constant and ≤ 1; and (iv) the liquid-solid interface is always perpendicular to the axis of the specimen. These conditions are believed to correspond closely to those encountered in pulsed-laser annealing in many instances. However, the formation of cellular structure in the distribution of some impurities has been observed in laser annealed samples[8,9]; and this is a clear indication that conditions ii and iv may break down.[10] It should be noted that condition iii does not specify whether k_i is an equilibrium (k_i^0) or a nonequilibrium value.

Smith *et al.* solve the dopant diffusion equation in the liquid, i.e.,

$$D_l \frac{\partial^2 C_l(x,t)}{\partial x^2} = \frac{\partial C_l(x,t)}{\partial t} \ . \tag{4}$$

The motion of the melt front generally makes this equation quite difficult if not impossible to solve analytically, but the solution simplifies considerably when the initial concentration of the solute is uniform, as assumed in Ref. 7. Then a transformation to a coordinate system moving with the melt front can be made and the equation

$$D_l \frac{\partial^2 C_l(x',t)}{\partial x'^2} + v\frac{\partial C_l(x',t)}{\partial x'} = \frac{\partial C_l(x',t)}{\partial t} \tag{5}$$

obtained. Here x' is measured relative to the position of the melt front. We are interested in those solutions of this equation which give the steady-state behavior of C_l and the initial and terminal transients; once C_l is known at the interface, C_s can be determined from Eq. (1). The terminal transient occurs when the melt front approaches the end of the sample (solidification completed) and it is of particular interest in laser annealing, as we shall see.

The steady-state solution of Eq. (5) occurs when $\partial C_l/\partial t = 0$. The boundary conditions can then be written as

$$C_l(x') = \begin{cases} C_0 & \text{at } x' = \infty \quad (6a) \\ C_0/k_i & \text{at } x' = 0 \ , \quad (6b) \end{cases}$$

and the solution is

$$C_l(x') = C_0 + C_0(q/k_i)\exp[-(v/D_l)x'] \tag{7}$$

with $q = 1 - k_i$. It can be seen from this equation that under steady-state conditions the distribution of the dopant in the liquid immediately in front of the interface falls off exponentially with x' until C_0 is obtained. The second boundary condition requires that, at the interface ($x' = 0$), $C_l(0)$ must be such that the concentration in the solid is exactly C_0, that is, from the definition of k_i

$$C_s = k_i C_l(0) = C_0 \ . \tag{8}$$

It should be noted that this equation states that the concentration of dopant incorporated into the solid

TABLE I. Values of k_i^0 and D_l from the literature and the results for k_i from Ref. 17 and the present calculations.

Dopant	k_i^0	D_l[a] (10^{-4} cm^2/sec)	D_l[b] (10^{-4} cm^2/sec)	k_i (Ref. 17)	k_i (This work)
B	0.8	2.4±0.7	3.3 ±0.4	. . .	0.9 −1.0
P	0.35	5.1±1.7	2.7 ±0.3	. . .	0.9 −1.0
As	0.3	3.3±0.9	. . .	1.00	0.9 −1.0
Sb	0.023	1.5±0.5	1.4 ±0.5	0.7	0.8 −1.0
Ga	0.008	4.8±1.5	0.66±0.5	0.2	0.15–0.3
In	0.0004	6.9±1.2	0.17±0.3	0.15	0.10–0.20
Bi	0.0007	. . .	. . .	0.4	0.25–0.42

[a]Reference 15. [b]Reference 16.

under steady-state growth is exactly C_0 and *does not* depend on velocity. Smith *et al.* give curves of $C_l(x')/C_0$ as a function of $(v/D)x'$ for $k_i=0.1$, 0.01, and 0.001.

The equation for the initial transient as a function of x (not x') as given in Ref. 7 is

$$\frac{C_s(x)}{C_0}=\frac{1}{2}\left\{1+\operatorname{erf}\left[\frac{[(v/D_l)x]^{1/2}}{2}\right]+(2k_i-1)\exp\left[-k_i q\left(\frac{v}{D_l}\right)x\right]\times\operatorname{erfc}\left[\frac{(2k_i-1)}{2}\sqrt{(v/D_l)x}\right]\right\}. \quad (9)$$

We will show plots of this equation for several values of k_i shortly. It should be noted from the definition of k_{eff} [Eq. (2)] that this equation can be thought of as giving an expression for a *transient component* of k_{eff} which is velocity dependent.

Smith *et al.* give an equation for the terminal transient which we will not repeat here since it is in series form and not particularly transparent. The series diverges at $x_2=0$ (x_2 is the distance from the front surface of the sample) if k_i is less than unity; however, for larger values of x_2 it converges quite rapidly. If $k_i=1$ (no segregation) there are, of course, no terminal or initial transients.

For illustrative purposes we have used the equations for the initial and terminal transients given in Ref. 7 to calculate the form of $C_s(x)/C_0$ for several different values of k_i. Except for $k_i=0.15$ these values correspond to the equilibrium interface segregation coefficients for B, As, Sb, and In in Si given in the compilation of Trumbore[11] (see Table I). The results are shown in Fig. 1 for a melt-front velocity of 4 m/sec and a typical diffusion coefficient of 4×10^{-4} cm^2/sec. It is obvious from this figure that, under typical conditions of pulsed-laser annealing, the segregation of some dopants may never reach the steady-state condition. Thus, for $k_i=0.15$, 0.023, and 0.0004, before the initial transient (solid line) is over, the melt front has reached the vicinity of the front surface where all of the dopant accumulated in the liquid ahead of the melt front is deposited by the terminal transient, as indicated by the dashed curves for $k_i=0.15$ and 0.023. We will discuss this feature again in the last section.

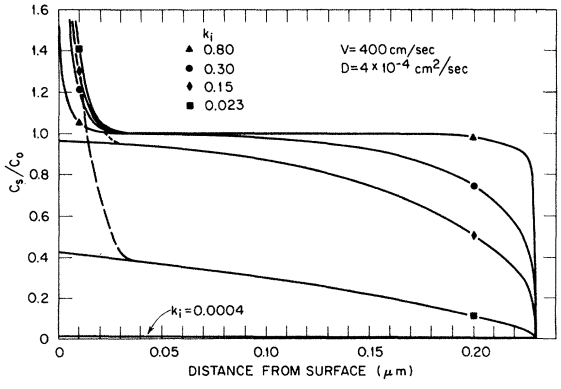

FIG. 1. The ratio of the dopant concentration C_s in the solid to that in the liquid of initially uniform dopant concentration C_0 as a function of distance from the surface. V and D are referred to as v and D_l in the text. The melt front was assumed to have penetrated to 0.23 μm and beyond this depth $C_s/C_0=1$, since no diffusion in the solid is allowed.

B. Segregation in a rotating crystal pulled from the melt

Burton, Prim, and Slichter[6] considered the case of segregation in a crystal pulled from melt with the crystal subjected to various rotation rates as in the well-known Czchrolski method. The liquid-solid interface in this case is approximately a plane disk and

the result of the rotational motion is to produce a component of fluid velocity normal to the disk. Equation (5) is modified for steady-state growth to

$$D_l \frac{d^2 C_l(x')}{dx'^2} - V(x') \frac{dC_l(x')}{dx'} = 0 \tag{10}$$

with $V(x') = v + W(x')$; $W(x')$ is the component of the fluid velocity induced by the rotation. Following an approximation by Cochran,[12] Burton *et al.* take

$$W(x') = 0.51 \omega^{3/2} \nu^{-1/2} x'^2, \quad x' < \nu^{3/2} \omega^{-1/2} \tag{11}$$

in which ω is the angular velocity of crystal rotation and ν is the kinematic viscosity. They obtain an approximate solution to Eqs. (10) and (11) at the interface given by

$$\frac{C_l(0) - C_s}{C_0 - C_s} = e^{\Delta} , \tag{12}$$

with $\Delta = v\delta/D$ and the quantity δ given by

$$\delta = 1.6 D^{1/3} \nu^{1/6} \omega^{-1/2} . \tag{13}$$

Equation (12) can be rewritten first as

$$C_s + [C_l(0) - C_s] e^{-\Delta} = C_0 \tag{14}$$

and then as

$$\frac{C_s}{C_0} = \frac{C_s}{C_s + [C_l(0) - C_s] e^{-\Delta}} \tag{15}$$

or

$$k_{\text{eff}} = \frac{k'}{k' + (1 - k') e^{-\Delta}} \tag{16}$$

with $k_{\text{eff}} \equiv C_s/C_0$ and $k' \equiv C_s/C_l(0)$. We emphasize again that k' can be either k_i^0 or k_i. Figure 2 shows k_{eff} as a function of v for several different values of ω in Eq. (13); ν and D were given the values used in Ref. 6. We see from Eq. (11) that when $\omega = 0$ the steady-state equation corresponding to Eq. (5) is recovered. In that case, $C_s = C_0$ and $k_{\text{eff}} = 1$ and it is apparent that the velocity dependence of k_{eff} in the Burton, Prim, and Slichter treatment is due entirely to the rotational motion which produces $W(x')$. This can also be seen from Eq. (13) which gives $\delta = \infty$ when $\omega = 0$, or, from Eq. (16), $k_{\text{eff}} = 1$. It is also indicated by the results on Fig. 2. The effect of the rotational motion is to draw liquid from the region far in front of the interface and well removed from the diffusion boundary layer. The concentration of the impurity in this liquid is much less than it is in the boundary layer region. The result is that less impurity is incorporated into the solid. When the rotation rate becomes very large, δ becomes very small and $k_{\text{eff}} \to k^0$. In this limit, liquid of low impurity concentration (C_0) is being brought into the interface region so quickly that the buildup of $C_l(0)$ substantially above C_0 cannot occur.

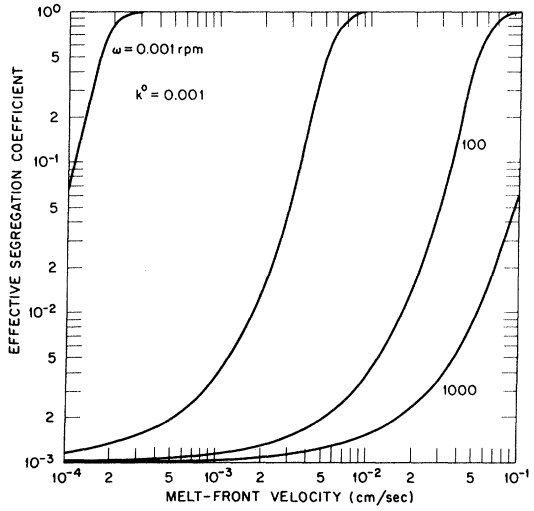

FIG. 2. The effective segregation coefficient of Burton, Prim, and Slichter as a function of melt-front velocity for several different values of the rotational velocity ω.

III. MODELS AND APPROXIMATIONS FOR DOPANT TRANSPORT CALCULATIONS

The thermal transport calculations in Paper I indicated that the near-surface region of the silicon sample melted during pulsed-laser annealing. The diffusion coefficients of most dopants in molten silicon (see Table I) are several orders of magnitude higher than they are in the solid and are quite large enough to explain the profile spreading that is observed after laser annealing. In this section, we discuss several approximations we have used to calculate the dopant redistribution. In all of these approximations, we assume that the thermal and mass diffusion problems can be effectively decoupled so that the heat transport results from Paper I become input data for the present calculations.

A. Instantaneous approximation (IA)

In those cases where the melt front penetrates well beyond the implanted dopant profile, rather good fits to the experimental data can be obtained by assuming that the region of the profile is instantaneously melted, stays molten for a certain period of time, and then is instantaneously resolidified. This "instantaneous approximation" (IA) involves a straightforward solution of Eq. (4) during the time the near surface region is molten; it also corresponds to an infinite melt-front velocity during melting and recrystallization. We have found it convenient to work in a Green's-function formulation in which the dopant profile in the solid after laser annealing is given by

$$C_s(x,t) = \int_0^{\infty} [G(x,t|x_0,t_0) C_i(x_0,t_0)]_{t_0=0} dx_0 , \tag{17}$$

where C_i and C_s are the initial ($x = x_0, t = t_0$) and final profiles, respectively, and $G(x,t|x_0,t_0)$ is the Green's function. If the melt front penetrates well beyond the region of the implanted profile, it is a good approximation to take $G(x,t|x_0,t_0)$ to be the Green's function for diffusion in a semi-infinite sample, i.e.,

$$G(x,t|x_0,t_0) = [4\pi D_l(t-t_0)]^{-1/2} \times \left[\exp\left[\frac{-(x-x_0)^2}{4D_l(t-t_0)}\right] + \exp\left[\frac{-(x+x_0)^2}{4D_l(t-t_0)}\right]\right] . \quad (18)$$

Because the melting and resolidification are assumed to occur instantaneously, C_i in the liquid is just the implanted profile in the solid and the final profile in the solid is the same as that in the liquid at the end of the melt time. C_i will generally be given in numerical form. It should be noted that the IA used here does not allow for segregation, i.e., $k_i = 1$.

B. Modified IA (MIA)

The IA is too restrictive in its treatment of the effects of melt-front motion. For example, when the melt front does not penetrate beyond the implanted profile, a single time during which the entire profile is allowed to diffuse cannot be assigned in even an approximately correct manner. Clearly, it is necessary to limit the time during which the dopant atoms in any volume element of the initial profile are allowed to diffuse to the time the volume element is molten. Figure 3 shows a set of melt-front profiles for one of the calculations to be described later. We note that the time each element of the near-surface region remains molten is easily extracted from the curves. For example for curve 1, the surface melts at 10 nsec after initiation of the laser pulse and stays molten until 100 nsec, so that it remains molten for 90 nsec. A simple approximation which gives surprisingly good results and yet remains within the spirit of Eq. (17) is obtained from the following procedure. The time $t_j - t_0 = \Delta t_j$ during which a thin layer at a depth x_j in the sample remains molten, as calculated from the melt-front profiles, is substituted into Eqs. (17) and (18) and the integrations over x_0 are carried out to find $C_s(x_j)$. The integration over x_0 is of course allowed to go over only that part of the material which is molten during Δt_j since only this material can act as a diffusion source for rapid diffusion. Thus, if the melt front does not penetrate entirely through the impurity profile, only that part of $C_i(x)$ which is in the molten zone will undergo diffusion (we continue to neglect any diffusion in the solid). This requires that the Green's function in Eq. (18) be modified to that for a slab of appropriate thickness or, more approximately, that $G(x,t|x_0,t_0)$ of Eq. (18) be restricted in the range of x and x_0 and suitably renormalized.

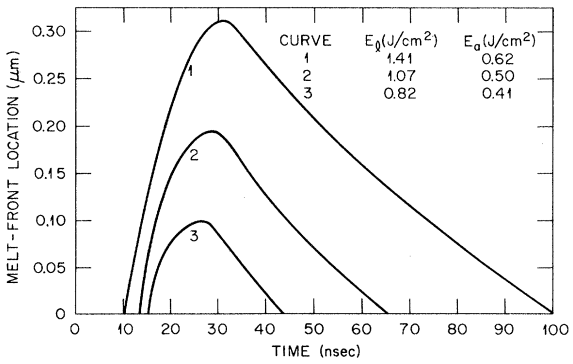

FIG. 3. Melt-front location as a function of time for a 100-keV As-implanted Si sample. E_I is the incident laser energy and E_a is the energy absorbed by the sample. Details of the calculation are given in the text and in Paper I.

C. Quasistationary finite-difference (QFD) approach

In the quasistationary approximation the sample is assumed to be divided into N layers or cells of various thicknesses. All of the material in any one layer melts or solidifies at the same time. The melt front thus advances into the solid and recedes back to the surface in finite jumps, and between jumps it is held stationary while diffusion in the molten material occurs. For example, beginning at the surface layer, the dopant diffusion equation is solved in that layer for some time interval and with the implanted profile as the starting profile. The melt front then jumps to the next layer where it pauses for a chosen time interval. During this interval, diffusion occurs with the initial profile given by the distribution of impurity in the first layer after the first time interval plus the implanted profile in the second layer. In this way, the diffusion equation is solved in steps as the melt front first penetrates into the sample and then returns to the surface. This problem can be solved analytically by using Green's functions appropriate to slabs of widths determined by the finite steps of the melt front. However, these Green's functions are given as infinite series and are rather cumbersome to work with. We have therefore used a quasistationary finite difference (QFD) approach which we now describe in some detail.

We let the bounding planes of the jth layer be x_j and x_{j+1} with $\Delta x_j = x_{j+1} - x_j$. In the finite difference algorithm we have followed, the dopant concentration at the center of a layer or computational cell is used. The diffusive fluxes $D(\partial C/\partial x)$ are defined at the

cell edges by

$$D(j)\left.\frac{\partial C}{\partial x}\right| = D(j)\frac{C(j+1/2)-C(j-1/2)}{x(j+1/2)-x(j-1/2)} \quad . \quad (19)$$

The subscripts have been placed in parentheses for convenience of printing, and subscripts indicating solid and liquid are not needed because the space and time indexing scheme together with the melt-front information determine whether solid- or liquid-state quantities are to be used. The flux approximation in Eq. (19) requires a diffusivity at x_j or, more exactly, an averaged diffusivity in the interval from $x(j-1/2)$ to $x(j+1/2)$. If the material is fully melted or fully solid in this interval, the choice of a value for D_j is straightforward; when the melt front is in the cell, the choice is more difficult. Generally, it is not desirable to move the mesh points to place the melt front in the center of a cell. Therefore, an averaged diffusivity for the interval which contains the melt front was determined using the reciprocal of the sum of the "resistances" to diffusion (i.e., $\Delta x/D$) in the subintervals containing the molten and the solid material. This approach has proved quite satisfactory in our calculations.

The boundary conditions assume that the flux through the front surface is known. In most experiments we will be concerned with, the surface flux is observed to be zero and the calculations reflect this condition; Sb and Ga in Si are exceptions to be described later. The boundary flux is added to the difference equation for the cell whose edge is the surface. The boundary condition used in the deep interior is one of zero flux; and, therefore, the mesh must be chosen to extend somewhat beyond the maximum depth that the melt front penetrates. Thus, the diffusion at the interior boundary is negligible so that the zero flux condition is as accurate as the more rigorously correct continuative condition.

The finite difference equation for an interior cell is

$$\frac{C(n+1;j+1/2)-C(n;j+1/2)}{\Delta t} = \frac{1}{\Delta x_j}\left[D(n+1;j+1)\frac{C(n+1;j+3/2)-C(n+1;j+1/2)}{x(j+3/2)-x(j+1/2)} - D(n+1;j)\frac{C(n+1;j+1/2)-C(n+1;j-1/2)}{x(j+1/2)-x(j-1/2)}\right] , \quad (20)$$

where the index $n+1$ represents quantities at time $t=(n+1)\Delta t$. The set of equations for the total assembly of cells becomes a system of simultaneous linear equations for the $C(n+1)$. This system is tridiagonal and may be solved by simple Gaussian elimination.

The modeling of segregation requires some significant alterations in the finite difference scheme described in the foregoing. The segregation process can be thought of as an internal "boundary" condition acting at the melt front to transfer dopant from the layer which is freezing to the immediately adjacent one which is still molten. Mathematically, the interface condition is given by Eq. (1). To deal with this internal condition, we chose to force the mesh to align with the melt front by creating extra cells at the beginning of each time cycle and then removing them at the end of the cycle. These small cells are inserted into the large cell which contains the melt front in such a way that the front is always at the center of one of the new cells. The interface condition is then applied to produce a "two-sided" (i.e., discontinuous) dopant distribution in the cell which contains the melt front. The modified finite difference equation for this cell is

$$\frac{C(n+1;j+1/2)-C(n;j+1/2)}{\Delta t} = \frac{1}{\Delta x_j}\left[\frac{D(n+1;j+1)}{x(j+3/2)-x(j+1/2)}\left(C(n+1;j+3/2)-\frac{2k_i}{k_i+1}C(n+1;j+1/2)\right) - \frac{D(n+1;j)}{x(j+1/2)-x(j-1/2)}\left(\frac{2}{k_i+1}C(n+1;j+1/2)-C(n+1;j-1/2)\right)\right] . \quad (21)$$

This assumes that the molten portion is at $x < x_{j+1/2}$. The two-sided nature of the dopant distribution at the interface is shown by the factors multiplying $C(n+1;j+1/2)$; we note that Eq. (21) reduces to Eq. (20) when $k_i=1$.

The implicit finite difference algorithm we have used is stable for any value of the time step Δt, but stability does not guarantee accuracy. For problems with no segregation, we found it necessary to limit the time-step size so that the melt front takes at least two cycles to cross a cell when the cell is resolidifying. For problems with segregation, the time-step limitations are more stringent. These limitations are dependent on the value of the segregation coefficient

and will be discussed below.

The accuracy of the computer code was first tested by comparison with the analytic solutions given in Sec. II. Not unexpectedly, numerical difficulties began to arise as the segregation coefficient was reduced from 1.0. Although the fully implicit diffusion algorithm is formally unconditionally stable, when diffusion and segregation are combined, instabilities can (and frequently do) occur. For example, in a calculation which allowed 26.5 time steps for the melt front to cross a 12.5-Å cell, the concentration in the solid developed a sawtooth pattern when k_i had the value 0.1. When the time step was cut in half, the sawtooth pattern vanished. With $k_i = 0.3$, the calculation with 26.5 time steps per 12.5-Å cell did not show the sawtooth instability.

In addition to stability, the time step also affects accuracy. For $k_i = 0.1$, the 53 time steps per cell needed for stability gave a concentration curve comparable to that given by the analytic solution using a value of $k_i = 0.15$. Reducing the time step by another factor of 8.0 (424 steps per 12.5-Å cell) gave a numerical solution which followed the analytical curve for $k_i = 0.12$. Results for a test case are shown on Fig. 4. Deviations of the calculated results from the analytic solutions approach zero as the time step goes to zero, but calculations with very small time steps can become prohibitively expensive. Calculations to test the effects of varying the time step were also run for $k_i = 0.3$ The calculation with 53 time steps per 12.5 Å cell gave a curve which followed the analytic curve for $k_i = 0.35$. Cutting the time step by another factor of 8.0 gave a curve which followed the analytic results for $k_i = 0.31$.

Our calculations with the QFD method have generally used a space step of 12.5 Å, but a few test calculations with $k_i = 0.1$ were run using a 6.25-Å step

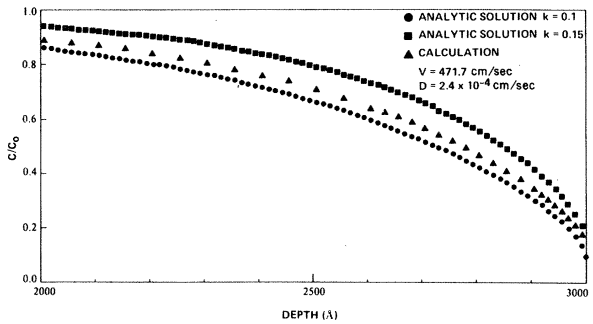

FIG. 4. An illustration of the difficulties encountered with the finite difference method for relatively small values of the interface segregation coefficient (denoted by k on this figure). The analytical solutions were obtained from Eq. (9) and the points labeled "calculation" were obtained from the QFD calculation. V and D are referred to as v and D_l in the text.

size. It was found that the results were virtually identical to those from calculations using the larger space step, provided one compared problems with time steps using the same number of cycles for the solid-liquid interface to cross a cell. In other words, when both space step and time step were cut in half, the results were virtually unchanged. This establishes that with these cell sizes the accuracy is controlled by the time step only, and thus, the 12.5-Å space step is quite sufficient. It is perhaps of interest to note that the magnitude of the spatial cells used here begins to approach interatomic dimensions in Si. The use of differential or difference equation to describe diffusion on a scale finer than we have employed becomes questionable.

D. Approximate treatment of segregation—MIAS method

The finite difference approach described above is capable of achieving great accuracy, and it can provide a high degree of flexibility, e.g., the diffusion coefficient can be allowed to depend on position and temperature. However, as we have seen, the computer time required to achieve acceptable accuracy increases very rapidly as the interface segregation coefficient decreases. To partially circumvent these drawbacks, we have developed an approximate approach based on the following model. The implanted profile is allowed to develop according to some approximation, e.g., the IA or MIA of this section. The profile is then fixed and segregation is allowed to occur as the melt front sweeps back through this profile. The concentration $C_l(j)$ in the liquid in the jth cell is made up of a contribution $C_{l,p}(j)$ from the diffused profile and a component $C_{l,\mathrm{seg}}(j)$ arising from segregation, i.e.,

$$C_l(j) = C_{l,p}(j) + C_{l,\mathrm{seg}}(j) \quad . \tag{22}$$

$C_{l,p}(j)$ is given from the first stage of the calculation and $C_{l,\mathrm{seg}}(j)$ is calculated by assuming that the dopant deposited just in front of the advancing melt front diffuses according to an exponential behavior, as one would expect for a steady-state problem. We have

$$C_{l,\mathrm{seg}}(j) = q \sum_{n=0}^{j-1} C_l(n) \left[\frac{v}{D_l}\right] \exp\left[-\left[\frac{v}{D_l}\right](x_j - x_n)\right] \Delta x_n \quad . \tag{23}$$

The nth term on the right side of this equation gives the contribution to the dopant concentration in the jth cell due to segregation of the dopant in the nth cell as the melt front sweeps through Δx_n. Equations (22) and (23) can be written in integral form as

$$C_l(x) = C_{l,p}(x) + q\left(\frac{v}{D_l}\right)\int_0^x C_l(x')\exp\left[-\left(\frac{v}{D_l}\right)(x-x')\right]dx' \quad . \tag{24}$$

We have carried out calculations with this expression for $C_l(x)$, but the presence of $C_l(x')$ in the integral is cumbersome and a simpler expression can be obtained as follows. Differentiate $C_l(x)$ to obtain

$$\frac{dC_l(x)}{dx} = \frac{dC_{l,p}(x)}{dx} - q\left(\frac{v}{D_l}\right)\left\{\left(\frac{v}{D_l}\right)\int_0^x \exp\left[-\left(\frac{v}{D_l}\right)(x-x')\right]C_l(x')\,dx' - C_l(x)\right\} \quad . \tag{25}$$

The last term comes from the upper limit on the integral in Eq. (24). Substituting Eq. (24) back into this expression gives

$$\begin{aligned}\frac{dC_l(x)}{dx} &= \frac{dC_{l,p}(x)}{dx} - \left(\frac{v}{D_l}\right)[C_l(x) - C_{l,p}(x)] + q\left(\frac{v}{D_l}\right)C_l(x) \\ &= \frac{dC_{l,p}(x)}{dx} + \left(\frac{v}{D_l}\right)[C_{l,p}(x) - k_i C_l(x)] \quad .\end{aligned} \tag{26}$$

This is a linear inhomogeneous equation which may be solved by standard methods. The result is

$$\begin{aligned}C_l(x) = &\left(\frac{v}{D_l}\right)\int_0^x \exp\left[-\left(\frac{v}{D_l}\right)k_i(x-x')\right]C_{l,p}(x')\,dx' \\ &+ \int_0^x \exp\left[-\left(\frac{v}{D_l}\right)k_i(x-x')\right]\frac{dC_{l,p}(x')}{dx'}dx' + C_l(0)\exp\left[-\left(\frac{v}{D_l}\right)k_i x\right] \quad .\end{aligned} \tag{27}$$

The second term on the right-hand side of this equation is zero if $C_{l,p}(x')$ is a constant C_0, and one finds that the distribution in the solid is given by

$$C_s(x) = k_i C_l(x) = C_0\{1 - q\exp[-k_i(v/D_l)x]\} \quad . \tag{28}$$

This equation was derived by Tiller *et al.*[13] on an intuitive basis and Smith *et al.* have shown that it is quite a good approximation to the correct form given by Eq. (9). When $C_{l,p}(x')$ is not constant the integrations in Eq. (27) can be carried out numerically. Equation (9) is an expression for the initial transient and does not give the segregation spike at the surface due to the terminal transient. This spike can be built into the calculations in an approximate but somewhat artifical manner. From Fig. 1 it is seen that the terminal transient is confined almost entirely to the region within 200 Å of the surface; and, since the experiments cannot give the dopant profile there reliably, it seems best just to deposit the final amount of segregated dopant in this region without undue concern for its exact distribution.

We have made extensive comparisons between the results given by Eq. (27) with $C_{l,p}(x')$ generated by our MIA and the results from the finite difference calculations. The differences between the results are invariably small; and with the uncertainties in the input data for the calculations and in the experimental data itself, it is virtually impossible at this time to claim that one method consistently gives a better fit to the experimental data than the other. Moreover, the predictions of the two methods are very nearly the same and it would seem, at this stage in the development of laser annealing, that highly accurate, expensive finite difference calculations are frequently not warranted. For simplicity, we will refer to the method described in this subsection as a modified instantaneous approximation with segregation, or MIAS for short.

IV. CALCULATIONS AND RESULTS

In this section we give the results of calculations by each of the methods described above but with particular emphasis on the methods in Secs. III B–III D. First, however, we demonstrate a simple method for scaling the melt-front profiles which are required as input for the dopant diffusion calculations.

A. Scaling of melt-front profiles

The thermal transport calculations described in Paper I can consume large amounts of computer time, and it is impractical to calculate melt-front profiles for every possible variation of laser energy density, pulse duration time, etc. Also, since there are uncertainties in the thermal conductivity, reflectivity before and after annealing, absorption coefficients, and other experimental quantities, some variation of melt-front profiles to improve the fit between calculated and experimental dopant profiles is justified. We will now describe a simple scaling procedure

which we have found useful in this connection.

Figure 3 shows a series of melt-front profiles obtained from calculations such as those described in Paper I for the "amorphous model." The calculations assumed an amorphous layer 0.15 μm thick had been created in the Si sample by the ion implantation of energetic heavy ions. In this region, the absorption coefficient was taken to be 5×10^4 cm^{-1} and in the deeper lying undamaged region of the sample it was assumed to be 3×10^3 cm^{-1}. The reflectivities of solid and molten Si were assumed to be 0.35 and 0.60, respectively. Further details of the model are given in I. We denote the melt-front location or depth as a function of time by

$$d_M = f(t) \tag{29}$$

and introduce a scale factor S. We then find that new melt-front profiles of very nearly the correct form are obtained by the simple scaling

$$d_M(St) = Sf(t) \ . \tag{30}$$

This scaling does not locate the melt-front profile on the time axis correctly, but in the dopant diffusion calculations we require only the duration of time that a layer at depth d_M remains molten; when the layer first began to melt is unimportant. Figure 5 shows how well the scaling procedure works. In this figure, we have used scaled melt-front profiles to plot the time that a layer at a given depth remains molten. The two dashed curves in Fig. 5 were constructed directly from curves 1 and 2 of Fig. 3, whereas the three solid ones were constructed from data obtained by scaling curve 1 of Fig. 3. The scale factor for the lowest solid curve on Fig. 5 was chosen to give very nearly the same maximum melt-front penetration as that of curve 2 on Fig. 3. The agreement between the lowest full and dashed curves on Fig. 5 is an indication of the success of the scaling procedure. Curves 1 and 2 of Fig. 3 were obtained with laser pulses of 1.41 and 1.07 J/cm^2, respectively, as indicated on the figure. We would not normally scale melt-front profiles over such large differences in the energy density and have done it in Fig. 5 only for illustrative purposes. This scaling technique should be used only within the framework of a given model. Models which differ widely from one another, e.g., when the thicknesses of the amorphous layers are greatly different, may have melt-front profiles which scale quite differently from one another.

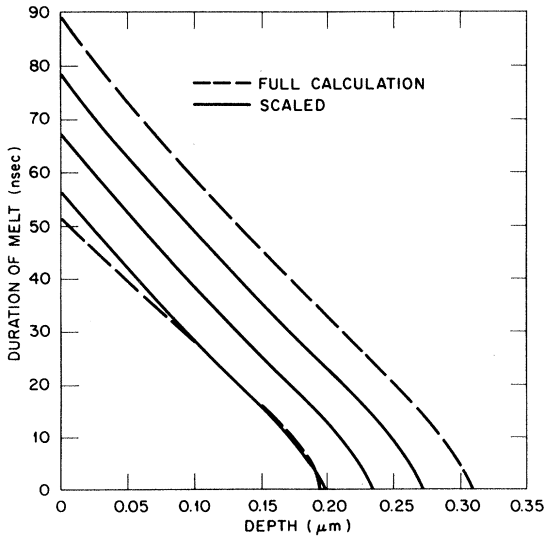

FIG. 5. Illustration of the results of scaling the melt-front profiles in Fig. 3 according to Eq. (30); see text for a discussion of the figure.

B. Input data

The only input data for these calculations are the initial dopant distributions, the melt-front profiles, dopant diffusion coefficients in molten Si, and the interface segregation coefficients. We have discussed the melt-front profiles above and in Paper I. The initial dopant distributions have generally been obtained by secondary ion mass spectroscopy[14] (SIMS) or by Rutherford backscattering[14] (RBS); they are supplied to the computer programs in numerical form. Two sets of values of D_l have appeared in the literature. We have generally used the set given by Kodera[15] because it is slightly more extensive than the one given by Shashkov and Gurevich[16] and gives better overall agreement between calculated and measured profiles. Both sets are shown in Table I. It should be noted that there are large differences in the two sets for a number of the dopants and that the error limits estimated by Kodera are quite large in some cases. Values of k_l^0 from the Trombore compilation, though shown in Table I, are not applicable to laser annealing and k_l was, in effect, taken as an adjustable parameter in the calculations to be described now.

C. Calculations with the IA and MIA

Figure 6 shows SIMS profiles of boron before and after laser annealing of a Si sample implanted with 35 keV $^{11}B^+$ to a dose of 1.03×10^{16}/cm^2. The annealing was carried out with a ruby laser using a pulse energy density of approximately 1.8 J/cm^2. The circles and squares give the experimental data before and after laser annealing, respectively. The solid curve marked with triangles was calculated by using the as-implanted profile (initial data) in the instantaneous approximation and varying the parameter $D * T$ [on Fig. 6, $D = D_l$ and $T = t - t_0$ in Eq. (18)] to obtain a satisfactory fit to the laser-annealed profile. With Kodera's value of D_l for boron from Table I, we find that

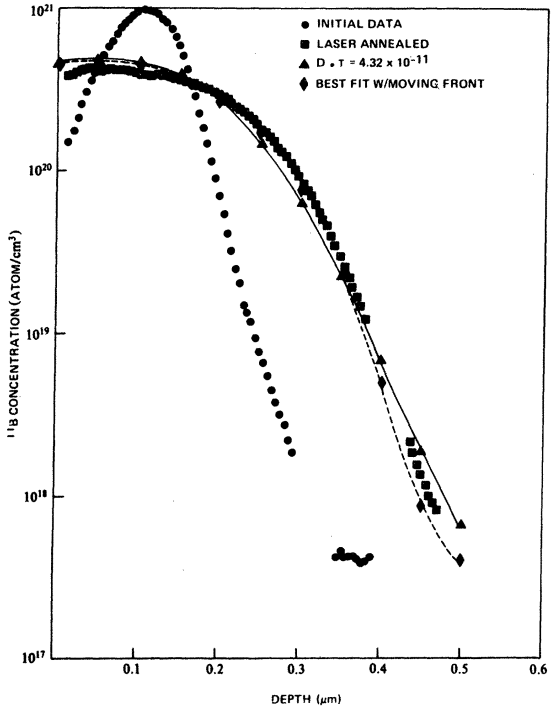

FIG. 6. Concentration of boron as a function of depth before and after laser annealing. The solid curve marked with triangles was calculated using the IA with the parameter $D * T$ (square of the diffusion length) varied to give the best fit to the experimental (initial) data; the dashed curve marked with diamonds was calculated by the QFD method. Both calculations assumed $k_i = 1$.

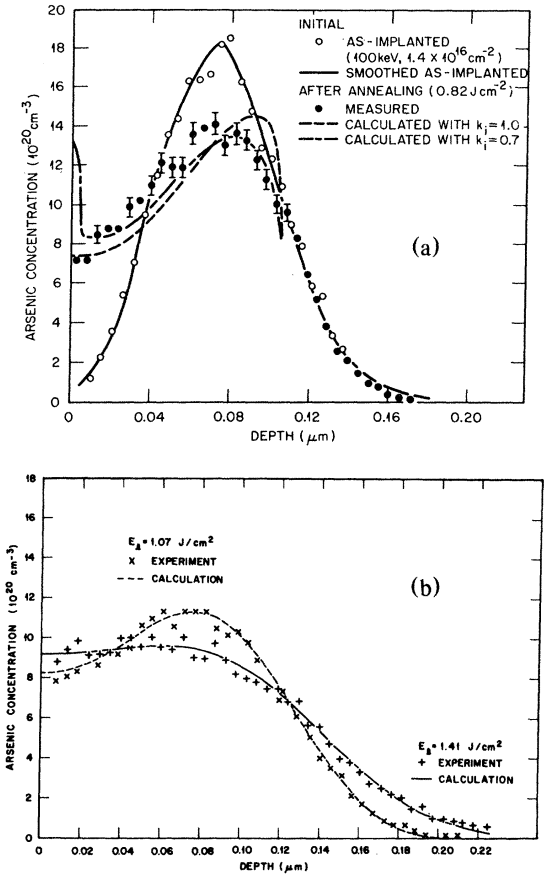

FIG. 7. (a),(b) RBS results for the dopant profiles in As-implanted Si. The as-implanted data for both figures are given on (a). The calculations were made with the MIA and MIAS methods. Further details are discussed in the text.

$T = 180$ nsec and with the Shashkov and Gurevich value, $T = 130$ nsec. These times are consistent with the time that a thin layer at a depth of ~ 0.40 μm remains molten after a 1.75–2.0-J/cm^2 ruby laser pulse (see, e.g., Fig. 4 of Paper I). Similar results were found for P, As, and Sb implanted samples but we will not show the results here. The lack of a concentration spike at the surface in the experimental data should be noted (see also Ref. 14). Because of the lack of such a spike, we took $k_i = 1$ for B, P, and As. There is some loss of dopant in the case of Sb but $k_i \simeq 1$, as we shall see below.

Figures 7(a) and 7(b) show the results of fitting arsenic profiles in As-implanted (100 keV, 1.4×10^{16} cm^2) Si samples with the modified instantaneous approximation. The experimental profiles were measured by RBS and the uncertainty in concentration at any given depth due simply to counting statistics is indicated on Fig. 7(a). The calculations were made with the melt-front profiles of Fig. 3 scaled slightly to improve the least-squares fit between experimental and calculated curves. The initial, as-implanted data were smoothed for the calculations, but subsequent testing showed that this smoothing made very little difference in the profiles after laser annealing. The segregation coefficient was put equal to unity in all but one of the calculations whose results are shown in Figs. 7(a) and 7(b). As mentioned above, the lack of any surface segregation peak argues for this choice. The overall agreement between experiment and calculations is quite good for Fig. 7(b); however, there is an interesting problem in connection with Fig. 7(a) which we now briefly discuss.

Figure 3 shows that for a laser pulse of 0.82 J/cm^2 the maximum melt-front penetration is approximately 0.1 μm. From Fig. 7(a), we can see that this implies that the melt front should not have penetrated all the way through the implanted profile, and indeed for the 0.82-J/cm^2 pulse the experimental profiles before and after laser annealing coincide at depths greater than ~ 0.1 μm. The calculations show that with $k_i = 1$ the profile should have the form shown by the indicated curve on Fig. 7(a); this curve does not fit the experimental profile as well as we might expect. We further refined the MIA to include segregation effects ap-

proximately (essentially in the manner described in Sec. III D) and carried out a calculation with $k_i = 0.7$. This calculation improved the agreement with experiment in the region around 0.1 μm, but it also gave a substantial segregation peak at the surface which is not observed. Quite similar results were obtained with the QFD method of Sec. III C. Since k_i^0 is 0.3 for As in Si (Table I), one suggestion from Fig. 7(a) is that we may be observing effects due to the transient buildup of k_i from 0.3 to 1.0. Before pursuing this line of investigation further with the calculations, it seems advisable to verify that the effect is real by further experimentation. Experiments using a dopant with k_i^0 smaller than 0.3 and with the laser pulse chosen so that the melt-front profile penetrates just beyond the peak of the implanted profile might enhance the effect.

The MIA was also used to fit dopant profiles obtained when As-doped layers of amorphous Si were deposited on Si substrates and then recrystallized by laser-induced melting.[3] The results for layers 0.1 and 0.2 μm thick are shown in Fig. 8. The experimental profiles were determined by anodic oxidation and stripping together with measurements of the electrical carrier concentration. The starting profiles cannot be measured by this technique because most of the As is electrically inactive when the deposited layer is still amorphous. However, the deposition conditions were such that the As concentration in the deposited layer should have been fairly uniform. The melt-front calculations were carried out with the same model described above (and in Paper I) to obtain the melt-front profiles of Fig. 3 but with the thickness of the amorphous layer changed to match the experimental conditions. The uniform concentrations required to give the calculated profiles are shown by the dashed lines on the figure.

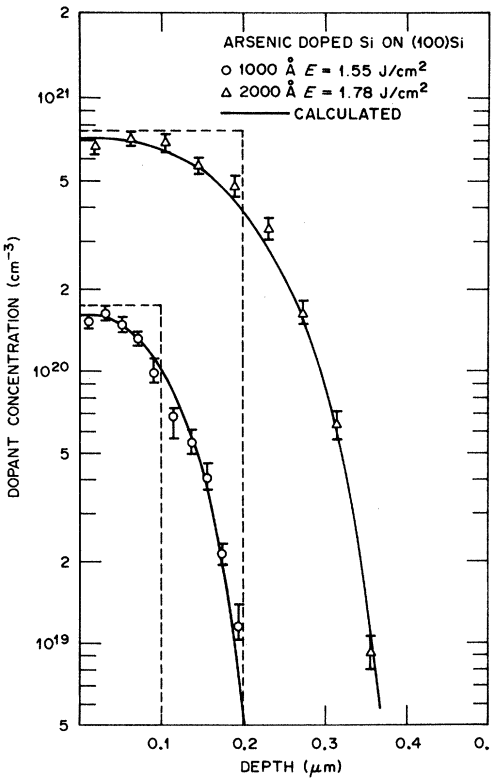

FIG. 8. Dopant profiles in Si samples on which As-doped amorphous layers 0.1 and 0.2 μm thick were deposited and subsequently laser irradiated at the energy densities indicated on the figure. The dashed curves are the assumed idealized starting profiles.

Perhaps it is worth emphasizing here that the basic thermal and dopant diffusion models used to obtain the results on Figs. 7(a), 7(b), and 8 are the same. Only the thickness of the amorphous layer, and therefore the melt-front profile, and the initial dopant distribution change in going from one calculation to another. Thus there is an internal consistency within the models and the calculations which argues strongly for the validity of the melting model of laser annealing.

D. Calculations with the QFD and MIAS methods

We first used the QFD method to calculate the boron profile of Fig. 6 and the dashed curve marked with ♦ shows the results. There is a definite improvement over the fit obtained with the IA. In qualitative terms, we believe this improvement comes about because the QFD method allows for the fact that the solidification front, as it moves back toward the surface, presents a barrier to further diffusion into the sample, thus steepening the annealed profile. A fit to the boron profile with the MIA gave a result nearly as good as that obtained with the QFD method but it is not shown on Fig. 6 to avoid a confusion.

Our most extensive use of the QFD and MIAS methods has been in fitting the data of White *et al.*[17] on Si implanted with Sb, Ga, In, and Bi. Unlike the results for B-, P-, and As-implanted laser-annealed Si, the profiles of Ga, In, and Bi in Si after laser annealing show clear evidence of segregation; the case of Sb is questionable, as we shall see. For Ga-, In-, and Bi-implanted samples, surface segregation spikes are observed, but they are not nearly as large as they would be if the values of k_i^0 shown in Table I were applicable. The necessity of choosing $k_i > k_i^0$ to obtain agreement between experimental and calculated profiles and the fact that the equilibrium solubility limit can be greatly exceeded as a result of the laser-annealing process[17,18] shows that the process is a highly nonequilibrium one. The nonequilibrium nature of laser annealing will be the subject of the third paper in this series. Here we will simply treat k_i as an adjustable parameter in the calculations. White *et al.* followed the same procedure in fitting their data

with calculations similar to our QFD and MIAS methods. Their calculations and ours were carried out totally independently, and the fact that the results are closely similar reinforces the basic validity of both sets of calculations.

E. Bismuth and indium

We discuss the Bi and In profiles first because, unlike Sb and Ga, they show no loss of dopant during laser annealing. The Bi was implanted at 250 keV to a dose of 1.2×10^{15} cm^{-2} and the In was implanted at an energy of 125 keV to the same dose. The laser annealing was done with laser pulses of $\sim$15 nsec duration full width at half maximum (FWHM) and $\sim$1.5-J/cm^2 energy density. The experimental results are shown in Figs. 9 and 10 for Bi and In, respectively. The calculations were carried out by first using the amorphous model (Paper I) to compute melt-front profiles for samples with amorphous layers of the appropriate thicknesses. These profiles were then taken as the starting melt-front data in the dopant diffusion calculations. The diffusion coefficients of Kodera were chosen and, as mentioned above, k_i was treated as an adjustable parameter. A limited amount of scaling of the melt front was used to improve the least-squares fitting of the experimental profiles. This fitting excluded the experimental points in the first 200 Å of the sample where the very large segregation spikes occur and where the data tend to have larger errors than elsewhere.

The results of Ref. 17 suggest that a good fit to the Bi data can be obtained with a value of k_i of 0.4 for a recrystallization velocity of 4.5 m/sec and a maximum melt depth of approximately 0.3 μm. A value of the diffusion coefficient for Bi in Si is not given by Kodera and the value used in the calculations of Ref. 17 is not specified. In our calculations with the QFD method, we assumed $D_l=2.4\times10^{-4}$ cm^2/sec. Minor scaling of the melt-front profile gave a maximum penetration depth of 0.360 μm instead of the 0.365 μm indicated by the heat transfer calculations for a 0.18-μm-thick amorphous layer; this difference is entirely inconsequential in view of the combined uncertainties in the experiments and calculations. The recrystallization velocity varies somewhat during the solidification process but an average velocity of 4.0–4.5 m/sec is indicated from the melt-front pro-

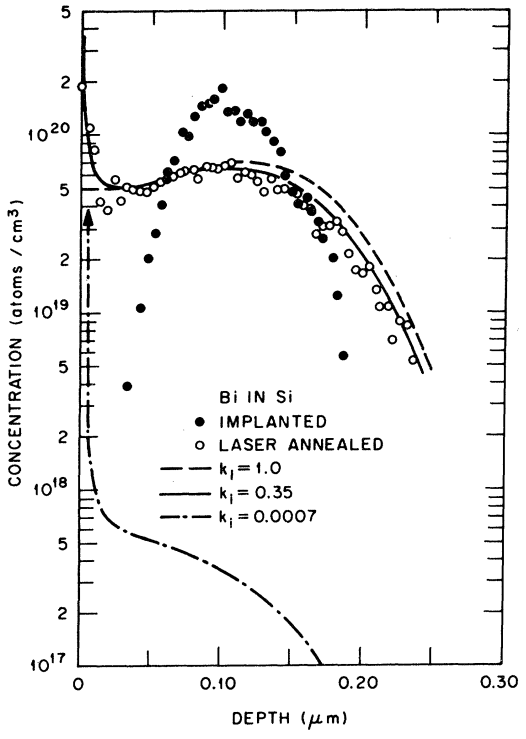

FIG. 9. Experimental (RBS) and calculated concentration profiles of Bi in Si after laser annealing. The implantation and laser-annealing conditions are given in the text. The total lack of a surface segregation peak for $k_i=1$ should be noted. The solubility limit of Bi in Si is $\sim8\times10^{17}$ atoms/cm^3.

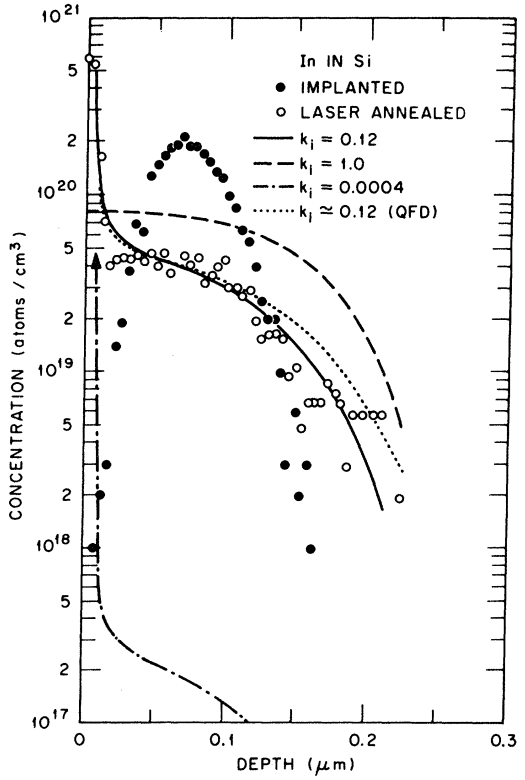

FIG. 10. Experimental and calculated concentration profiles of In in Si after laser annealing. For reasons explained in the text, the curve for $k_i=1.0$ is not the best fit when no segregation is allowed. The solubility limit of In in Si is $\sim8\times10^{17}$ atoms/cm^3.

files. We carried out calculations with $k_i = 1.0$, 0.5, 0.3, and 0.1 and found that $k_i = 0.3$ gave the best fit to the experimental data. Because of the convergence problems of the QFD method, we estimate that this corresponds to a true best value of $k_i \simeq 0.35$. The Bi profile for this value is shown on Fig. 9 by the solid line. Also shown on the figure is the profile for $k_i = 1.0$, i.e., with no segregation and the profile using the equilibrium value of $k_i^0 = 0.0007$; the latter is clearly unable to give a satisfactory fit to the experimental data. On a semilogarithmic plot such as Fig. 9, the differences between profiles with $k_i = 1.0$, 0.5, and 0.3 in the regions away from the surface peak do not appear very great. Therefore, an examination of the amount of dopant segregated to the surface region (depth $\simeq 200$ Å) is quite useful and the results reinforce our confidence in the model calculations. The experimental data show that of the implanted dose (1.2×10^{15} cm^{-2}) approximately 0.22×10^{15}/cm^2 or 18% is located within the first 190 Å of the surface; this includes the few points which lie in front of the surface in the experimental data (see Ref. 17). The corresponding percentages from the QFD calculations are 6, 11, 15, and 31 for k_i values of 1.0, 0.5, 0.3, and 0.1, respectively. Thus, both the percentage of dopant in the surface peak and the least-squares fitting of the dopant profile (which excludes the surface peak) with the QFD method indicate a value of k_i in the range 0.25–0.35. We were not entirely satisfied with the results of fitting the Bi data with the QFD method. As we have already discussed, the method has convergence problems unless one can afford the large amounts of computer time required when the time step is made very small. Therefore, we carried out a series of calculations, with the MIAS method, which is extremely fast. For these calculations, we assumed D_l values of both 2.4×10^{-4} and 4.4×10^{-4} cm^2/sec. The best fit to the smooth part of the experimental data was found for $k_i = 0.42$ and $D_l = 4.4 \times 10^{-4}$ cm^2/sec. This fit gave 18.4% of the dopant in the surface peak which is in remarkably close agreement with the experimental value of 18%. When $k_i^0 = 0.0007$ was used in the calculations, greater than 99% of the dopant was segregated to the surface.

The calculations on In in Si were carried out almost entirely with the MIAS method because the low value of k_i would have necessitated large amounts of computer time if the QFD method had been used extensively. We took $D_l = 6.9 \times 10^{-4}$ cm^2/sec from Table I, a maximum melt depth of 0.2975 μm and a recrystallization velocity of 4 m/sec. Figure 10 shows the results of the calculations. The best fit was obtained with $k_i = 0.12$ which is quite close to the value of 0.15 found in Ref. 17. The curve indicated for $k_i = 1$ may be somewhat misleading since it is not the best fit when no segregation is allowed. It is instead the profile which was used with $k_i = 0.12$ to generate the segregation calculation, as explained in Sec. III D. If we had put $k_i = 1$ and allowed the melt front to penetrate deeper, we could have obtained a better fit than that shown on Fig. 10, but there would still be no surface spike. A calculation with $k_i \simeq 0.12$ using the QFD method gave the dotted curve on Fig. 10; the calculation with $k_i^0 = 0.0004$ using the MIAS method is also shown on the figure. If we again consider the amount of dopant segregated to the surface (in the MIAS calculations), we find 61% which, as in the case of Bi, is remarkably close to the value of 60% obtained experimentally. This should be compared to the value of very nearly 100% when $k_i^0 = 0.0004$ is used in the calculation.

F. Antimony and gallium

The fitting of the profiles of these dopants in silicon presents an additional problem because there is a measurable loss of dopant during laser annealing under the conditions used in Ref. 17. We concentrated on the Sb results and made three different assumptions about dopant loss. In one set of calculations, all of the dopant loss occurred during the initial part of the surface melting when the temperatures in the liquid Si were the highest. Equally good fits to the experimental data were found for k_i values of 1.0 and 0.8. However, when the same assumption was applied to the case of Ga in Si satisfactory fits could not be obtained. A second set of calculations was carried out with the assumption that dopant loss occurred only when the surface concentration exceeded some threshold value. This assumption gave quite good fits to both the Sb and Ga experimental data but the fit for Sb required a value of $k_i = 0.4$ and a

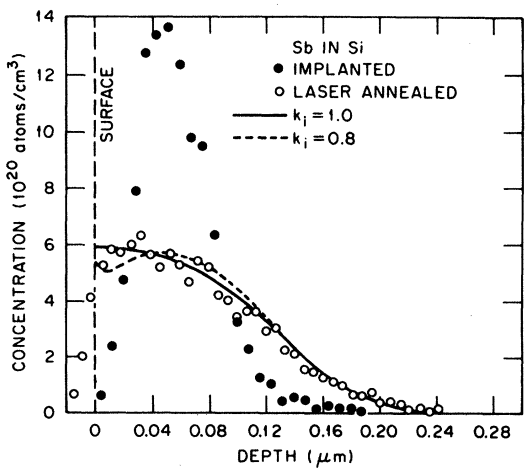

FIG. 11. Antimony distribution in Sb-implanted Si before and after laser annealing. There is some loss of Sb from the sample during laser annealing, as discussed in Ref. 17. The solubility limit of Sb in Si is $\sim 7 \times 10^{19}$ atoms/cm^3.

maximum melt-front penetration substantially less than indicated by the heat transfer calculations. In the third set of calculations, we used the approximation that the dopant loss is proportional to the surface concentration, as one would expect from a simple kinetic rate theory approach. We found that satisfactory fits to both Sb and Ga in Si could be obtained with this method. Although the rms deviations between experimental and calculated profiles for both dopants were not quite as good as those obtained with the assumption of a threshold concentration for dopant loss, the values of the maximum melt-front penetration needed to obtain the fits were much more in accord with the values given by the heat transfer calculations of Paper I (and the values used for the As, Bi, and In calculations). Figure 11 shows the results for Sb in Si from the third set of calculations. Our calculated results for Ga in Si are quite comparable to those reported in Ref. 17 and are not shown here.

V. DISCUSSION AND CONCLUSIONS

We view the results for B, P, As, In, and Bi in Si as being fairly unambiguous when the melt front penetrates beyond the as-implanted dopant profiles. Under similar circumstances, the experimental results for Sb and Ga are somewhat more difficult to interpret because the loss of dopant adds another variable to the modeling and calculations. However, even in these two cases the simplest and most natural physical assumption (dopant loss proportional to the surface concentration) leads to results most consistent with the thermal calculations of Paper I.

Several things must be kept in mind when evaluating the results of our calculations and the experiments. First, it should be recognized that Rutherford backscattering, though a very powerful and quantitative technique, yields fairly substantial error bars associated with the individual data points, unless one has the luxury of accumulating vast counting statistics. Our calculations have utilized rms fittings to the data as though no errors were involved. If these error bars had been taken into consideration, it would be virtually impossible to differentiate between a k_i of 1.0 and 0.9 for fitting the As data for example or between k_i values of 0.25–0.45 for fitting the smooth part of the data in Bi. Counterbalancing this are the precise results that both the experiments and the calculations give about the percentage of dopant contained in the surface spike. As we have seen, there is good agreement between experiment and theory on the percentage of dopant in this spike and this percentage is remarkably consistent with the results of the rms fitting of the smooth part of the profile.

Turning to the calculations, we see from Eqs. (7) and (9) of Sec. II that the ratio of v/D_l enters into the analytical solutions for the case that the initial dopant profile is constant. The heat transport and melting calculations of Paper I can be assumed to give fairly accurate values of v. The values of D_l however are subject to fairly large uncertainties as indicated by the error estimates of Kodera and the differences between Kodera's values and those of Ref. 16. In this connection, we carried out calculations on both Bi and In using the values of D_l from Ref. 16 and found the results totally unacceptable unless we greatly changed the melt-front profiles from those dictated by the heat transfer calculations of Paper I. We are convinced therefore that a reasonable and probably extremely useful way to proceed is to employ whatever means available to ascertain that the calculations of melt-front profiles give reliable results and then to use these profiles in the dopant diffusion calculations to determine the diffusion coefficients and the values of k_i. For example, as shown in Paper I, melt-front profiles generated by our calculations give results quite consistent with the duration of surface melting obtained by Auston *et al.*[19] from transient reflectivity measurements. We have then found from the calculations reported in this paper that the diffusion coefficients given by Kodera must be reasonably reliable. Systematic experimental studies of laser annealing coupled with refined calculations of melt-front profiles and further experiments and calculations on dopant redistribution can be expected to lead to improved values of both D_l and k_i. The last two columns in Table I show the values of k_i from the calculations of Ref. 17 and our best estimates from the calculations reported here. When the various sources of possible error in the experiments and calculations are considered, there is essentially complete agreement between the two sets of calculations.

The sketchy experimental results presented thus far on those cases in which the melt front does not penetrate entirely through the implanted profile may point the way toward a deeper understanding of the dynamics of ultrarapid crystallization. Data from such experiments can potentially lead to an understanding of the transient regime in which the recrystallization velocity builds up from zero to the high velocities characteristic of laser annealing. These transients are superimposed on those transients inherent in growth at a constant velocity illustrated in Fig. 1. It will require high instrumental resolution and a combination of careful experimentation and realistic modeling to disentangle these transients, but in principle it may be possible. The capability of treating both types of transients is already built into the QFD approach. A more important effect of the transients may come into play in the interpretation of experiments in which the dependence of k_i on melt-front velocity (see, for example, Ref. 18) is studied. As we have already noted, Fig. 1 shows that for

$k_i \leq 0.15$, a steady-state situation is not attained before the melt front reaches the surface. Thus the amount of dopant contained in the surface peak is not determined entirely by k_i, as it is when a steady-state situation exists. When the melt-front velocity is reduced (e.g., by substrate heating) to the point that k_i falls below about 0.15, it will be necessary to correct for the effect of the initial transient on the amount of dopant segregated to the surface before the true dependence of k_i on v can be determined. It is possible that such a correction should have been made here for the In results.

Closely connected with the above considerations are the problems of nonequilibrium segregation ($k_i \neq k_i^0$), how, when, and to what extent the equilibrium solubility limit is exceeded, and the breakdown of the planar melt front to produce the cellular structure observed in laser-annealed semiconductors.[8,9] These questions, which will be addressed in the third paper of this series, are among the most important and fascinating ones in modern materials science and solid-state physics. Pulsed laser annealing for the first time provides a flexible and reliable technique for studying ultrarapid recrystallization phenomena and their consequences. Calculations of the type discussed in this paper and Paper I must form an integral part of such studies.

We end this paper by taking note of the fact that the recent experiments of Lo and Compaan[20] on Raman scattering during pulsed-laser annealing have been interpreted as implying that the near-surface region of the sample does not melt. The experiments of Lo and Compaan are important but also difficult to perform and interpret. They were carried out with a laser that gave heating pulses only 90 μm in diameter, and the spatial homogeneity of the pulses, which we know to be of vital importance, over such small areas could not be studied. In contrast to this one result that seems to imply that melting does not occur, there is a large body of experimental data on transient reflectivity, dopant redistribution, cellular formation, etc., which, gives very strong evidence that melting does occur. We believe that the excellent fits which we have obtained here between experiments and calculations based on the melting model make it extremely difficult to seriously question the basic validity of the melting hypothesis. It would be a truly remarkable coincidence if a nonmelting hypothesis could lead to a theory (yet to be constructed) which duplicated virtually all of the results of the melting model.

ACKNOWLEDGMENTS

We would like to thank F. W. Young, Jr. for his careful reading of the manuscript and the authors of Ref. 17 for access to their data before its publication. This research was sponsored by the Division of Materials Sciences, U.S. Department of Energy under Contract No. W-7405-eng-26 with the Union Carbide Corporation.

---

*Computer sciences division.

[1]R. F. Wood and G. E. Giles, Phys. Rev. B 23, 2923 (1981).

[2]J. C. Wang, R. F. Wood, and P. P. Pronko, Appl. Phys. Lett. 33, 455 (1978); J. C. Wang, R. F. Wood, C. W. White, B. R. Appleton, P. P. Pronko, S. R. Wilson, and W. H. Christie, in *Laser-Solid Interactions and Laser Processing—1978,* edited by S. D. Ferris, H. J. Leamy, and J. M. Poate, AIP Conf. Proc. No. 50 (AIP, New York, 1979); R. F. Wood, G. E. Giles, and J. R. Kirkpatrick, in *Laser Applications in Materials Processing,* edited by J. F. Ready (Society of Photo-Optical Instrumentation Engineers, Bellingham, 1980), Vol. 198, p. 2; R. F. Wood, J. C. Wang, G. E. Giles, and J. R. Kirkpatrick, in *Laser and Electron Beam Processing of Materials,* edited by C. W. White and P. S. Peercy (Academic, New York, 1980), p. 37; G. E. Giles, J. R. Kirkpatrick, and R. F. Wood, paper 80-HT-13 (American Society of Mechanical Engineers, New York, 1980); AIAA paper 80-1473 (American Institute of Aeronautics and Astronautics, New York, 1980).

[3]R. T. Young, J. Narayan, and R. F. Wood, Appl. Phys. Lett. 35, 447 (1979).

[4]See, for example, in *Moving Boundary Problems,* edited by D. G. Wilson, A. D. Solomon, and P. T. Boggs (Academic, New York, 1978).

[5]See, for example, Refs. 2, 3, 14, and 17.

[6]J. A. Burton, R. C. Prim, and W. P. Slichter, J. Chem. Phys. 21, 1987 (1953).

[7]V. G. Smith, W. A. Tiller, and J. W. Rutter, Can. J. Phys. 33, 723 (1955).

[8]G. J. van Gurp, G. E. Eggermont, Y. Tamminga, W. T. Stacy, and J. R. M. Gijsbers, Appl. Phys. Lett. 35, 273 (1979).

[9]J. Narayan, J. Met. 32, 15 (1980).

[10]W. W. Mullins and R. F. Sekerka, J. Appl. Phys. 35, 444 (1964).

[11]F. A. Trumbore, Bell Syst. Tech. J. 39, 205 (1960).

[12]W. G. Cochran, Proc. Cambridge Philos. Soc. 30, 365 (1934).

[13]W. A. Tiller, K. A. Jackson, J. W. Rutter, and B. Chalmers, Acta Metall. 1, 428 (1953).

[14]C. W. White, J. Narayan, and R. T. Young, Science 204, 461 (1979).

[15]H. Kodera, Jpn. J. Appl. Phys. 2, 212 (1965).

[16]Y. M. Shashkov and V. M. Gurevich, Russ. J. Phys. Chem. 42, 1082 (1968).

[17]C. W. White, S. R. Wilson, B. R. Appleton, and F. W. Young, Jr., J. Appl. Phys. 51, 738 (1980).

[18]R. F. Wood, Appl. Phys. Lett. 37, 302 (1980).

[19]D. H. Auston, J. A. Golovchenko, A. L. Simons, R. E. Slusher, P. R. Smith, C. M. Surko, and T. N. C. Venkatesan, in *Laser-Solid Interactions and Laser Processing—1978,* edited by S. D. Ferris, H. J. Leamy, and J. M. Poate, AIP Conf. Proc. No. 50 (AIP, New York, 1979).

[20]H. W. Lo and A. Compaan, Phys. Rev. Lett. 44, 1604 (1980).